



Hybrid precast tunnel segments in fiber reinforced concrete with glass fiber reinforced bars

Alberto Meda^a, Zila Rinaldi^{a,*}, Simone Spagnuolo^a, Benoit De Rivaz^b, Nello Giamundo^c

^a University of Rome Tor Vergata, Rome, Italy

^b BMUS, Aalst, Belgium

^c ATP, Angri, Italy

ARTICLE INFO

Keywords:

Tunnel segments
Hybrid solution
Fiber reinforced concrete
Glass-fiber reinforced bars
Full-scale tests

ABSTRACT

The interest in using fiber reinforced concrete (FRC) for the production of precast segments in mechanical excavated tunnel lining is continuously growing, as witnessed by the studies available in literature and by the actual applications. The possibility of adopting a hybrid solution of FRC tunnel segments with Glass Fiber Reinforced Polymer (GFRP) reinforcement is investigated herein. The proposed solution can cover the situations in terms of requirements that cannot be satisfied with the FRC solution only. On the same way the use of GFRP bars can avoid the problems related to the use of traditional steel rebars. A typical metro tunnel geometry is considered, and full-scale segments are designed, cast and experimentally validated. In particular, one flexural and one point load full-scale tests are carried out, for the evaluation of the structural performances (both in terms of structural capacity and crack pattern evolution) of tunnel segments with hybrid solution, under bending, and under the TBM thrust. The experimental behaviors are compared with the ones obtained on fiber reinforced only segments, with the same geometry and concrete material. Finally, the obtained results are discussed, and the effectiveness of the proposed technical solution, in increasing the bending resistance and, mainly in reducing the crack width under flexural and TBM thrust, is highlighted.

1. Introduction

The introduction of the mechanically excavated tunnels technology, through a tunnel boring machine (TBM), and the following advantages in terms of costs and construction times, has given a great spread of interest in the design, safety check, and actual application of the precast segments composing the tunnel lining. Furthermore, this peculiar application lends itself to innovation in terms of materials and structural systems. In the last few years the adoption of fiber reinforced concrete (FRC) in precast tunnel segments, has encountered a great interest, as witnessed by theoretical and experimental studies (Plizzari and Tiberti, 2008; Caratelli et al., 2011; Coccia et al., 2015; Liao et al., 2015; Di Carlo et al., 2016), and actual applications (Kasper et al., 2008; De La Fuente et al., 2012; Caratelli et al., 2012). The solution of FRC elements, without any discrete reinforcement, provides the great advantages, in terms of cost and precast production (fib Bulletin 83, 2017). Nevertheless, in some part of the tunnel, for particularly loading condition (typically under prevalent bending actions, as in cross-passage or shallow tunnel), the FRC only solution cannot satisfy the requirement. In this case, two solutions are possible: (a) to increase the

FRC performance or (b) to adopt a hybrid solution adding rebars. Since the first solution is sometime problematic due to necessity to qualify another material, the second solution can be more realistic.

However, in this latter case, the problems related to the tunnel lining durability, with particular reference to steel rebar corrosion, also due to possible induced stray current, can be critical (fib Bulletin 83, 2017), and the use of non-metallic rebars combined with FRC could be an alternative solution.

The possibility of adopting glass fiber reinforced polymers (GFRP) reinforcement in precast tunnel segments in ordinary concrete was investigated by some of the authors in previous papers (Caratelli et al., 2016; Caratelli et al., 2017; Spagnuolo et al., 2017, 2018).

GFRP bars in concrete structures can be proposed as an alternative to the traditional steel rebars, mainly when a high resistance to the environmental attack is required. Indeed, GFRP reinforcement does not suffer corrosion problems and its durability performance is a function of its constituent parts (Micelli and Nanni, 2004; Chen et al., 2007). From the mechanical point of view, the GFRP bars are characterised by an elastic behavior in tension, and, with respect to the steel ones, present higher tensile capacity, lower elastic modulus, and lower weight (Nanni

* Corresponding author at: University of Rome "Tor Vergata", Via del Politecnico, 1, 00133 Rome, Italy.

E-mail address: rinaldi@ing.uniroma2.it (Z. Rinaldi).

1993; Benmokrane et al., 1995; Alsayed et al., 2000). The compression strength is often neglected, due to its low value. GFRP is also electrically and magnetically non-conductive, but sensitive to fatigue and creep rupture (Almussalam et al., 2006). Furthermore, the structural effects of the low elastic modulus and bond behavior (Cosenza et al., 1997; Yoo et al., 2015; Coccia et al., 2017) have to be considered. Due to all these aspects, this type of reinforcement is not suitable for all applications, but it appears appropriate for tunnel segments, both for provisional and permanent elements.

In order to evaluate the synergic effect of the above mentioned composite materials, tunnel segments made in FRC and reinforced with GFRP bars were cast and experimentally tested. This hybrid solution can be very useful in tunnel lining for the aforementioned reasons.

No references are available on the proposed solution for the peculiar application in tunnel segments, but some studies are present in literature dealing with the combination of fiber reinforced concrete – fiber reinforced polymers reinforcement (FRC-FRP). The problem of the bond behavior has been analysed, through experimental tests in (Wona et al., 2008; Kim et al., 2013; Ding et al., 2014). The influence of the fibers on the flexural behavior and ductility of concrete beams reinforced with FRP bars was experimentally studied by (Issa et al., 2011; Wang and Belarbi, 2011; Yang et al., 2012; Qin et al., 2017). The results show the advantages of the hybrid system in improving the flexural performances, increasing the ductility level, and reducing the crack widths.

Finally, Wang and Belarbi (2013) studied the durability of FRC beams reinforced with FRP bars, by accelerated aging tests. The obtained results indicated that the ultimate flexural strength and ductility experienced minor reduction when exposed to combined environmental conditioning, including freeze–thaw cycles, high temperature (60 °C), and de-icing salt solution.

Aim of the paper is the evaluation of the structural performances of tunnel segments with hybrid solution (FRC reinforced with a perimetric GFRP cage) through full-scale experimental tests. One flexural and one TBM tests were carried out and the results were compared with the ones obtained on fiber reinforced specimens. The effectiveness of the solution, mainly in reducing the crack width both for flexural loading and TBM thrust action, is finally highlighted.

2. Segment geometry and materials

Four full-scale fiber reinforced concrete segments were cast and subjected to bending and point load tests. The specimens presented a geometry typical of metro tunnels with external diameter of 6400 mm, characterized by a thickness of 300 mm, and a width of about 1400 mm (Fig. 1). Two of the four segments were further reinforced with a perimetric GFRP cage, as specified in the following.

2.1. Fiber reinforced concrete

The segments were cast in moulds available at the Laboratory of the University of Rome Tor Vergata (Fig. 2), equipped with electrical vibrators to compact the concrete, prepared in a track mixer.

The concrete mix design is shown in Table 1. Steel fibers Bekaert Dramix 4D 80/60BG (length and diameter equal to 60 mm and 0.75 mm, respectively, tensile strength equal to 1800 MPa) were added with a content of 40 Kg/m³.

The average compressive strength of the fiber reinforced material measured on 6 cubes having 150 mm side, was equal to 62.35 MPa.

The tensile behavior was characterized through bending tests on nine 150 × 150 × 600 mm notched specimens according to the EN 14651. The diagrams of the nominal stress versus the crack mouth opening displacements (CMOD) are plotted in Fig. 3. Furthermore, in Table 2 are summarised the values of the stress related to the proportionality limit (f_l) and the residual nominal strengths related to four different crack openings - CMOD (0.5, 1.5, 2.5 and 3.5 mm), named f_{R1} , f_{R2} , f_{R3} , f_{R4} , as suggested by the Model Code 2010 (fib, 2013).

Both the tests for the characterization of the material in compression and tension were carried out after 30 days from casting, at the same time of the full-scale tests.

2.2. GFRP cage

Two fiber reinforced segments, named SFRC-GFRP, were further reinforced with a perimetric Glass Fiber Reinforced Polymeric (GFRP) cage made with interlinked closed-rings (longitudinal/transversal), as shown in Fig. 4. This solution, obtained through a suitable manufacturing technology, based on a modified pultrusion able to produce curvilinear and closed ring bars with a constant and large curvature radius (Caratelli et al., 2017), facilitate the cage assembly operation. The longitudinal and transversal rings are connected with wires.

The GFRP bars have a nominal diameter of 16 mm, and are characterized by physical and mechanical properties shown in Table 3.

The glass fiber reinforcement was suitably designed - according to the CNR-DT203 guidelines (CNR, 2007) for GFRP bars and Model Code 2010 (fib, 2013) for the fiber reinforced concrete - in order to provide an increase of the ultimate bending moment of about 50%, with respect to the SFRC (steel fiber reinforced concrete) section. The adopted bars layout in the cage is typical of hybrid solutions, with the longitudinal reinforcement working for flexural actions (Fig. 4a and b). The transverse reinforcement is placed for keeping the position of the longitudinal bars, only, and not for structural reason.

3. Segment test set-up

One flexural and one point-load tests were carried out, for both the SFRC (fiber reinforced segments without any discrete reinforcement) and SFRC-GFRP segments, as discussed in detail in the following. In particular, both flexural and point load full-scale tests were carried out, for the evaluation of the structural performances (both in terms of structural capacity and crack pattern evolution) under bending, and under the TBM thrust.

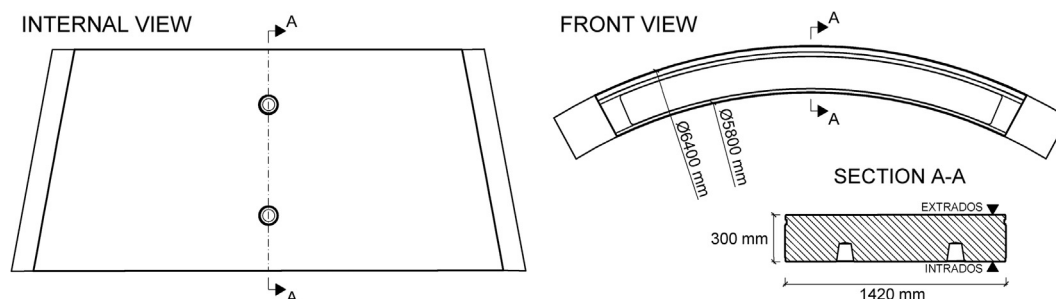


Fig. 1. Segment geometry.



Fig. 2. Segment cast and curing.

Table 1
Concrete mix design.

Component	kg/m ³
Cement 42.5 R	480
Natural sand (0–4 mm)	422
Crushed sand (0–4 mm)	423
Crushed aggregate (4–16 mm)	519
Crushed aggregate (16–25 mm)	350
Plasticiser	4.8
Water	170
Steel fiber	40

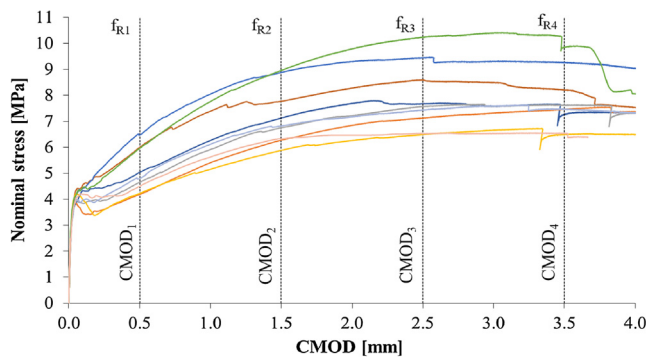


Fig. 3. Results of the beam bending tests.

Table 2
Results of the beam bending tests.

Dosage [kg/m ³]	Specimen ID	f _L	Residual flexural tensile strength			
			f _{R1}	f _{R2}	f _{R3}	f _{R4}
			[MPa]			
40 kg/m ³	B1	3.85	5.03	7.12	7.67	7.25
	B2	4.34	5.99	7.77	8.60	8.20
	B3	4.14	6.47	8.88	9.44	9.26
	B4	3.91	4.18	6.27	7.12	7.46
	B5	4.10	4.65	6.75	7.57	7.62
	B6	4.21	4.22	5.88	6.50	6.48
	B7	4.15	5.96	8.97	10.24	9.86
	B8	3.91	4.80	6.82	7.43	7.45
	B9	4.03	4.49	6.32	6.52	6.54
Average		4.07	5.09	7.20	7.90	7.79
Std. Dev		0.50	0.84	1.12	1.28	1.14
CV		4%	17%	16%	16%	15%

3.1. Bending test

The bending tests were performed with the loading set-up illustrated in Fig. 5, in displacement control, by adopting a 4000 kN hydraulic jacket.

The segments were placed on cylindrical support with a span of 2000 mm and the load, applied at midspan, was transversally distributed by adopting a steel beam as shown in Fig. 5.

The load was measured by means of a 1000 kN load cell. The midspan displacements were measured with three potentiometer wire transducers placed along the transverse line (Fig. 6), while the displacements at the midspan intrados surface were measured with two LVDTs (Fig. 6). Furthermore, the crack pattern was recorded at different steps, with the help of a grid plotted on the intrados surface (100 × 100 mm), and the crack widths were measured with a crack gauge.

3.2. Point load test

The point load test was performed by applying three-point loads at the segment and adopting the same steel plates used by the TBM machine (Fig. 7). A uniform support is considered, as the segment is placed on a stiff beam suitably designed (Meda et al., 2016). Every jack, having a loading capacity of 2000 kN, is inserted in a close ring frame made with HEM 360 steel beams and 50 mm diameter Dywidag bars (Fig. 7). The load was continuously measured by pressure transducers. Six potentiometer transducers (three located at the intrados and three at the extrados) measure the vertical displacements, while two LVDTs transducers are applied between the load pads. (Fig. 7). Furthermore, during the tests, the widths of the formed cracks were measured with a crack gauge (Fig. 7c).

4. Bending test results

The results of the bending tests are summarised in this section.

4.1. SFRC segment

The displacements measured by the three wire transducers (Fig. 6) are plotted versus the load in Fig. 8. The maximum load was about 225 kN.

The first cracks appeared for a load value of about 125 kN, at the lateral surfaces close to the midspan of the segment and propagates on the intrados.

The segment at the end of the tests is shown in Fig. 9, and the detected crack pattern is summarised in Fig. 10.

In Fig. 11 the LVDTs displacements are plotted versus the load. It is worth noting that two cracks pass through the instruments lengths (Fig. 10), and then the measure is related to the total strain and to the sum of their crack widths.

Finally, with reference to the crack numbering of Fig. 10, the crack widths measured with the crack gauge, for each load step, are summarised in Table 4.

4.2. SFRC-GFRP segment

The results obtained for the FRC segment reinforced with the GFRP

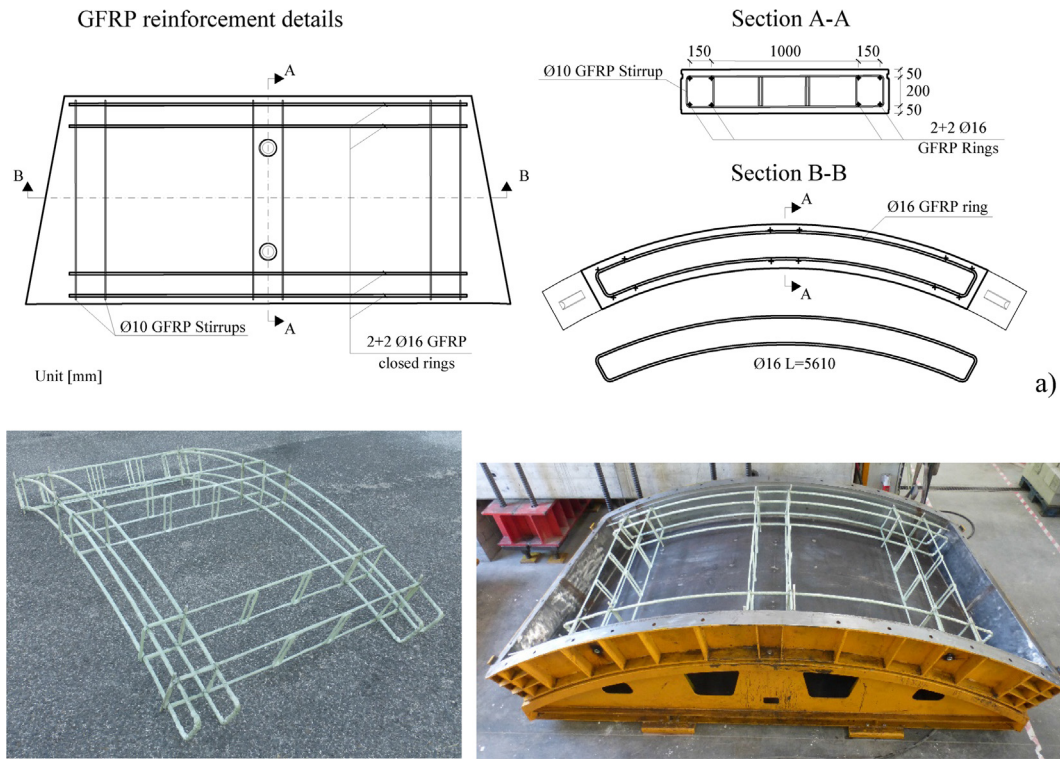


Fig. 4. (a) GFRP segment geometry; (b) GFRP cage.

Table 3
Physical and mechanical properties of GFRP bars.

Physical properties	Unit	Value	Test method
Equivalent cross-sectional area	mm ²	191	ASTM D792
Equivalent diameter	mm	15.6	ASTM D792
Density of the fiber (E-CR Glass)	g/cm ³	2.62	–
Density of the resin (Vinyl ester)	g/cm ³	1.15–1.35	–
Glass content	% volume	68	NRC DT203
Mechanical properties			
Young's modulus	GPa	46	ASTM D7205
Tensile strength	MPa	983	ASTM D7205

cage are summarised through a load-displacement diagram in Fig. 12. The maximum load was about 367 kN.

The first cracks appeared for a load value of about 120 kN, at the lateral surfaces close to the midspan of the segment and propagates at the intrados.

The state of the segment at the end of the test is highlighted in Fig. 13, while the detected crack pattern is summarised in Fig. 14.

In Fig. 15 the LVDTs displacements are plotted versus the load. It is worth noting that two cracks pass through the instruments lengths (Fig. 14), and then the measure is related to the total strain and to the sum of their crack widths.

Finally, with reference to the crack numbering of Fig. 14, the crack widths measured with the crack gauge, for each load step, are

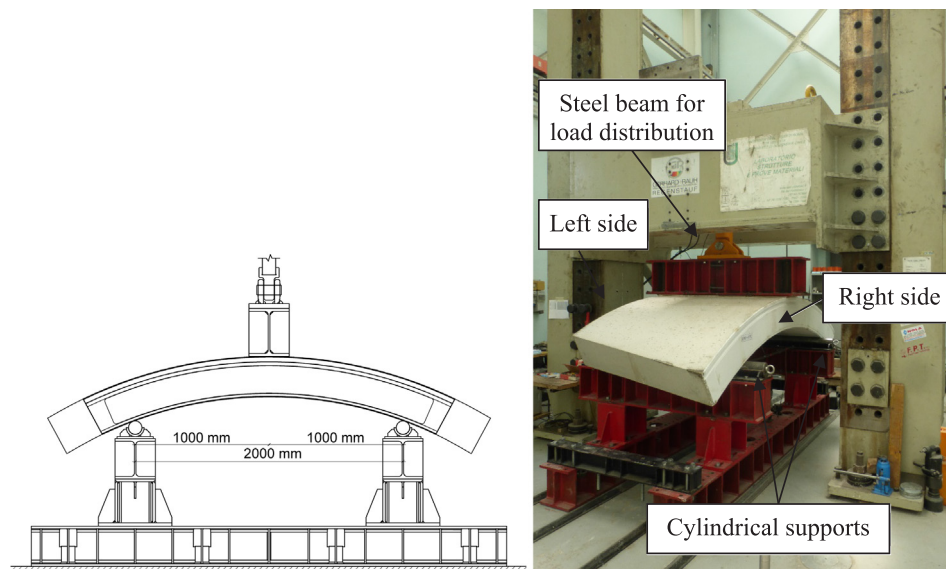


Fig. 5. Bending testing set-up.



Fig. 6. Bending test instrumentation.

summarised in Table 5.

4.3. Flexural tests: Comparison

The behavior of the segments SFRC and SFRC-GFRP are finally compared in Fig. 16, where the average value of the displacement, measured by the three potentiometer wires, are plotted versus the load.

It can be noted that, after a first comparable almost elastic response, the SFRC-GFRP segments present a peak load about 63% higher than the SFRC one.

The maximum crack widths, measured at different load steps, are compared in Table 6. The obtained results clearly show the synergic effects of the two materials in reducing the crack widths, with respect to FRC solution, of about 60%.

5. Point load test results

The loading process for the segments under point-load test is highlighted in the following. The chosen reference load levels equal to 1580 kN and 2670 kN for each pad refer to the service load and un-blocking thrust of the TBM machine. For the SFRC segments two cycles were performed, as highlighted in Fig. 17a, through the load – time diagram.

For the SFRC-GFRP segments, to better enquire the influence of the GFRP reinforcement on the crack width and mainly on the crack reclosing, four cycles were carried out, and two further intermediate load levels were introduced. The load – time diagram is shown in Fig. 17b.

The effectiveness of the testing set-up was verified by the instrument devices: no rotation of the segment was detected by the potentiometer transducers (Fig. 7c), and similar tensile deformations were measured by the two LVDTs (Fig. 7a and c), between the loading pads.

5.1. SFRC segment

The final crack pattern, after the point load test, is shown in Fig. 18 and the crack widths, measured with a crack gauge during the test, are reported in Table 7.

The first cracks appeared for a load level of 1250 kN (for each steel pad) between two pads at the top and lateral surfaces (Fig. 18). The crack width was lower than 0.05 mm. This crack propagated in the following step (1580 kN) at the intrados surface, as highlighted in Fig. 18. The maximum crack width was about 0.1 mm. According to the adopted loading history (Fig. 17a), the complete unloading followed and the cracks appeared completely reclosed (see Table 7). For a load level of about 2500 kN a bursting crack opened under a point load (see Fig. 18), at both the intrados and extrados sides. The maximum crack



Fig. 7. Point load test and instrumentation: (a) Intrados surface; (b) Extrados surface; (c) detail of the potentiometer transducers, LVDT device and crack gauge.

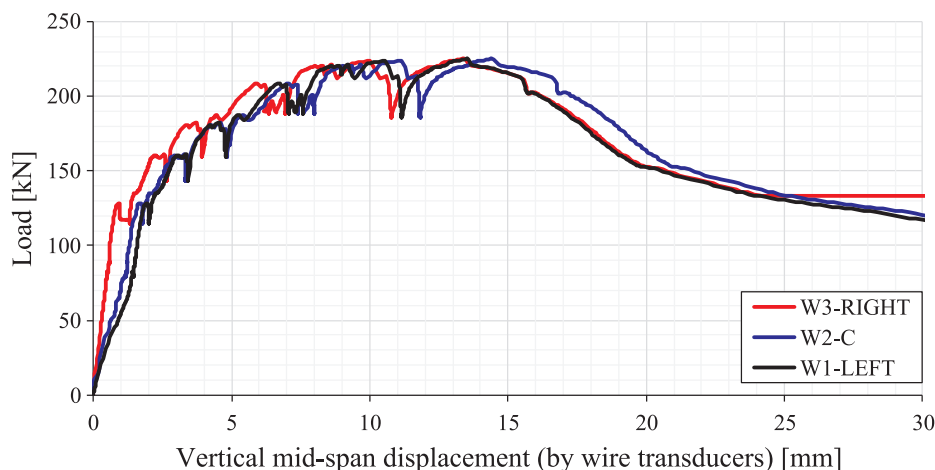


Fig. 8. SFRC segment. Bending test: load-mean displacement curve.

width, measured with a crack gauge, was equal to about 0.35 mm. For the load values of 2670 kN, corresponding to unblocking thrust, the maximum crack width was equal to 0.40 mm (Table 7). At the end of the test, after the complete unloading, the maximum crack width was about 0.15 mm.

5.2. SFRC-GFRP segment

The final crack pattern after the point load test is shown in Fig. 19 and the crack widths measured during the test are reported in Table 8.

The first cracks appeared for a load level of 1250 kN (for each steel pad) between two pads at the top and lateral surfaces (Fig. 19). The crack width was lower than 0.05 mm. Further two cracks formed for the load level of 1350 kN at the top surface (Fig. 19). The maximum crack

width was lower 0.05 mm (Table 8). According to the adopted loading history (Fig. 17b), the complete unloading followed and the cracks appeared completely reclosed. The same cracks re-opened in the second cycle up to 1350 kN, with a maximum crack width lower than 0.05 mm. (see Table 8). For a load level of 1580 kN, a small lengthening of the already formed cracks appeared at the intrados side. According to the adopted loading history (Fig. 17b), the complete unloading followed and the cracks appeared almost completely reclosed (See Table 8).

In the third cycle new small crack opened for a load level of 2000 kN, while for a load level of 2250 kN, besides splitting cracks between the steel pads, a bursting crack, also, opened under one point load (Fig. 19), at both the intrados and extrados sides. In the last fourth cycle new cracks opened for load values of 2500 kN and 2670 kN (Fig. 19). The maximum crack width, for the maximum load was equal

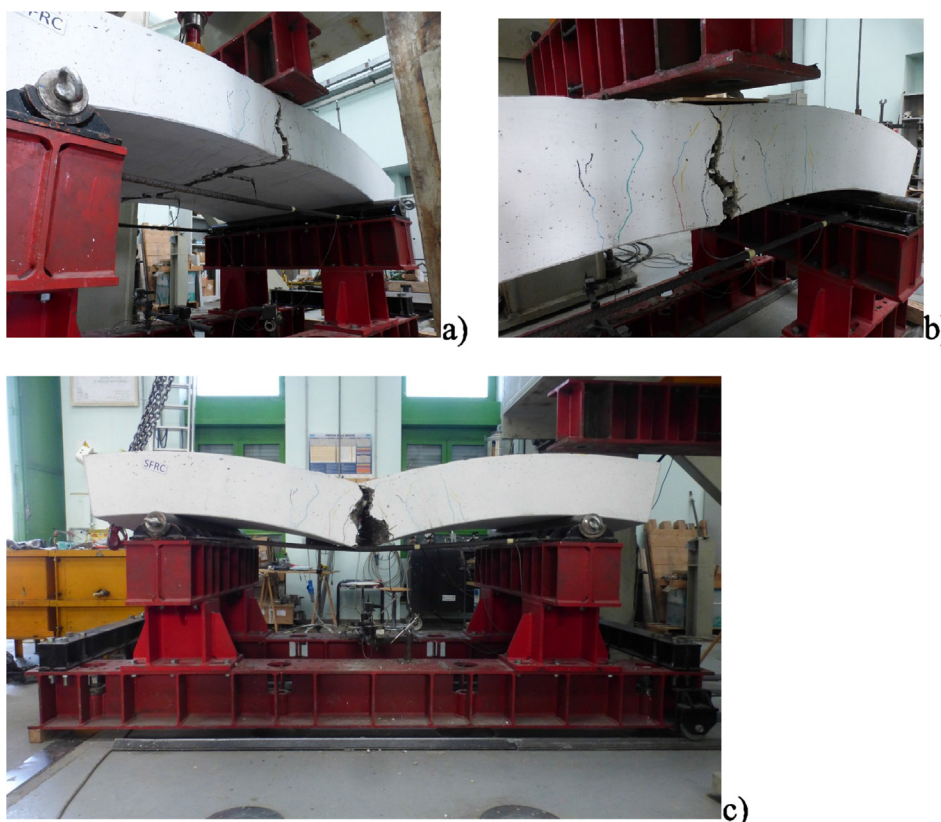


Fig. 9. SFRC segment: Bending test. End of the test: (a) Intrados surface; (b) Failure detail; and (c) Thrust side.

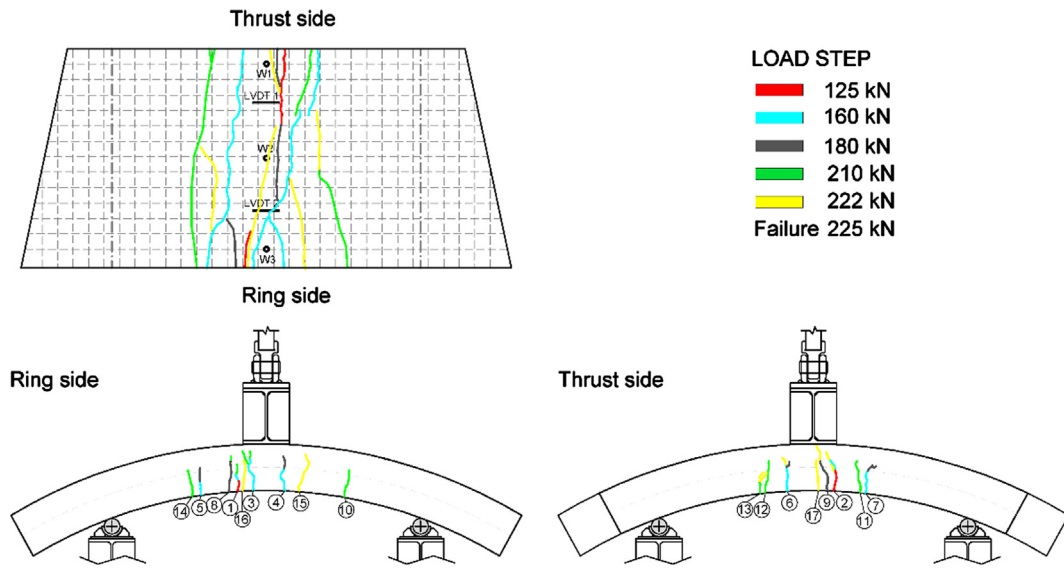


Fig. 10. SFRC segment: Bending test. Crack pattern.

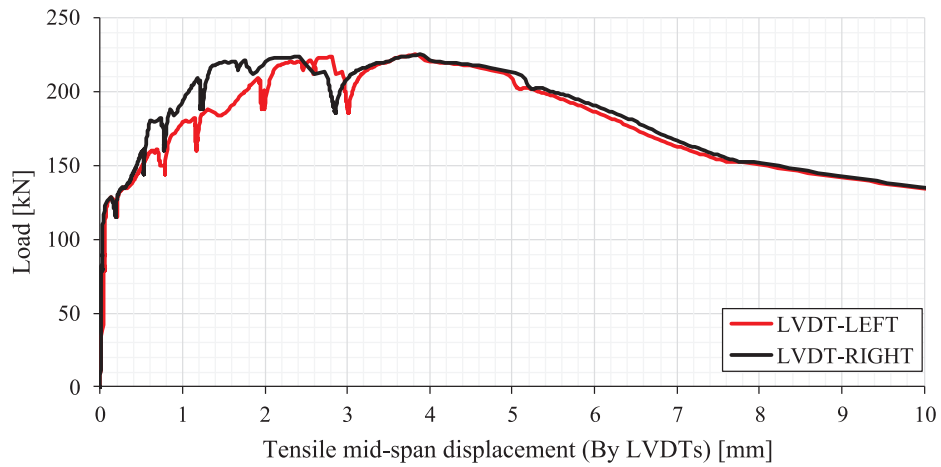


Fig. 11. SFRC segment. Bending test: LVDTs measures.

Table 4
SFRC segment. Bending test: measured crack widths.

Load [kN]	Loading					225 P _{max}
	125	160	180	210	222	
Crack colour						
Crack n.	Crack width [mm]					n/a
1	<0.05	0.05-0.10	0.10	0.30	0.40	
2	<0.05	0.25	0.35	0.35-0.40	0.70	
3	-	0.20	0.35	0.60	1.00	
4	-	0.10-0.15	0.30-0.35	0.45	0.70	
5	-	0.05	0.10	0.15	0.35-0.40	
6	-	0.10-0.15	0.20-0.25	0.30	0.30	
7	-	<0.05	0.15	0.15	0.15	
8	-	-	0.15	0.30	0.40	
9	-	-	0.10-0.15	0.40	0.90	
10	-	-	-	0.20	0.30	
11	-	-	-	0.40	0.60	
12	-	-	-	0.20	0.20	
13	-	-	-	0.05	0.20	
14	-	-	-	0.15	0.15	
15	-	-	-	-	0.60	
16	-	-	-	-	0.05	
17	-	-	-	-	0.40	

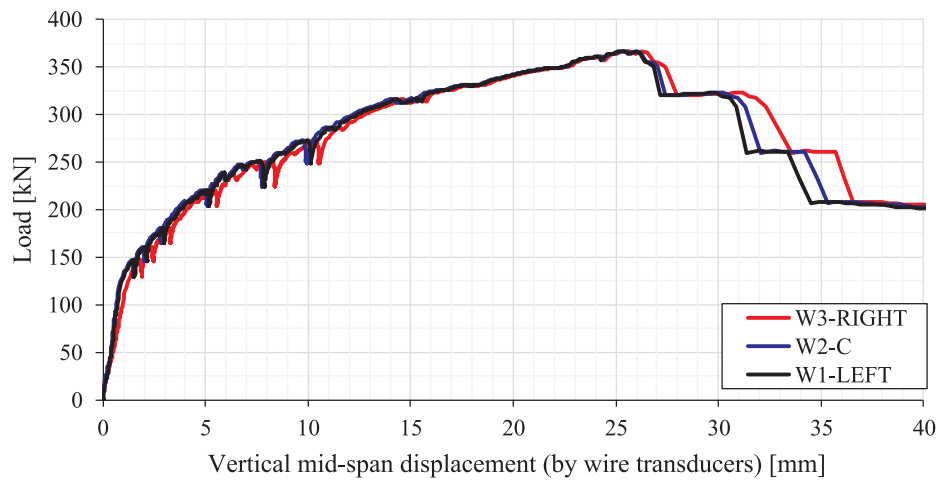


Fig. 12. SFRC-GFRP segment. Bending test: load-mean displacement.

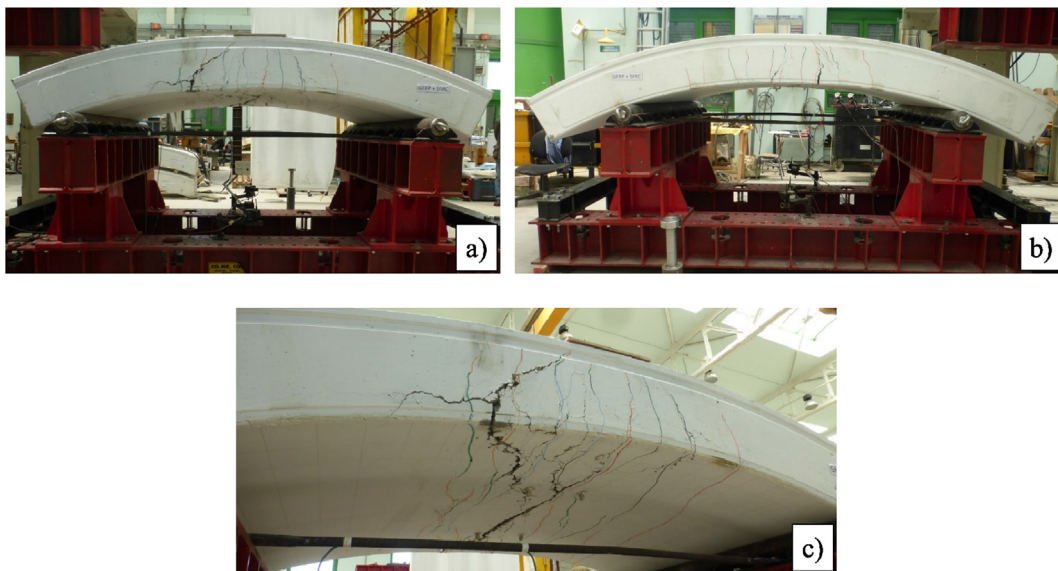


Fig. 13. SFRC-GFRP segment: Bending test. End of the test. (a) Thrust side; (b) Ring side; and (c) Intrados surface.

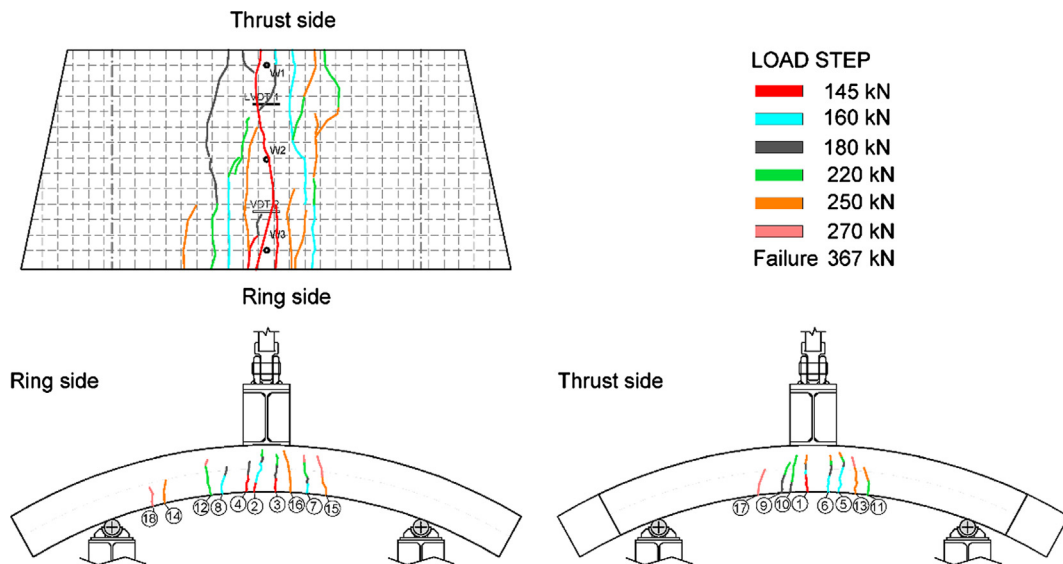


Fig. 14. SFRC-GFRP segment. Bending test: Crack pattern.

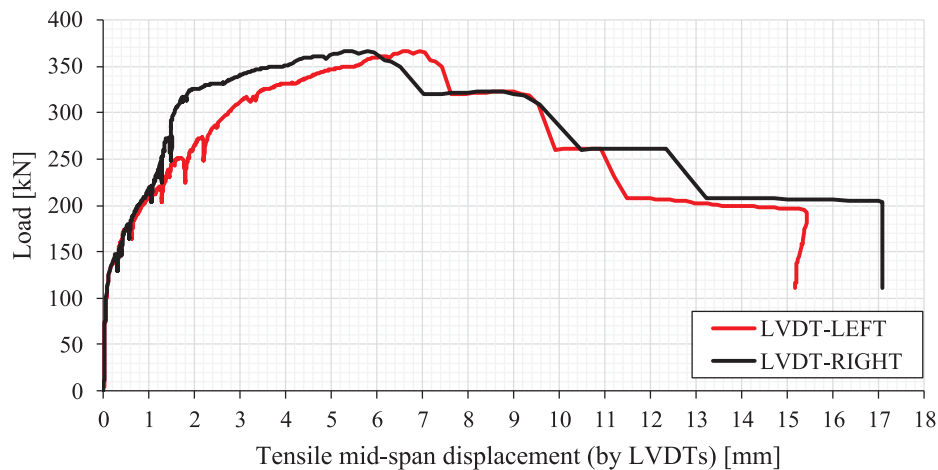


Fig. 15. SFRC-GFRP segment. Bending test: LVDTs measures.

Table 5
Segment SFRC-GFRP. Bending test: measured crack widths.

Load [kN]	Loading						P _{max}
	120	160	180	220	250	270	
Crack colour	Red	Blue	Black	Green	Orange	Brown	P _{max}
Crack n.	Crack width [mm]						
1	<0.05	0.05-0.10	0.15	0.25	0.40	0.70	
2	<0.05	<0.05	0.10	0.3-0.35	0.35	0.30	
3	<0.05	0.10	0.10-0.15	0.25	0.35	0.35	
4	<0.05	<0.05	0.05	0.10	0.30	0.30	
5	-	0.10	0.15	0.20	0.15-0.20	0.15	
6	-	0.05	0.15	0.30-0.35	0.35	0.60	
7	-	<0.05	0.10	0.20	0.30	0.25	
8	-	<0.05	0.05-0.10	0.15	0.20	0.15	
9	-	-	0.05	0.15	0.20-0.25	0.30	
10	-	-	<0.05	0.10	0.10	0.10	n/a
11	-	-	-	0.05	0.20	0.25	
12	-	-	-	0.10	0.15	0.25	
13	-	-	-	-	0.15	0.15	
14	-	-	-	-	0.05	0.15-0.20	
15	-	-	-	-	<0.05	0.10	
16	-	-	-	-	0.45	0.60	
17	-	-	-	-	-	0.05	
18	-	-	-	-	-	<0.05	

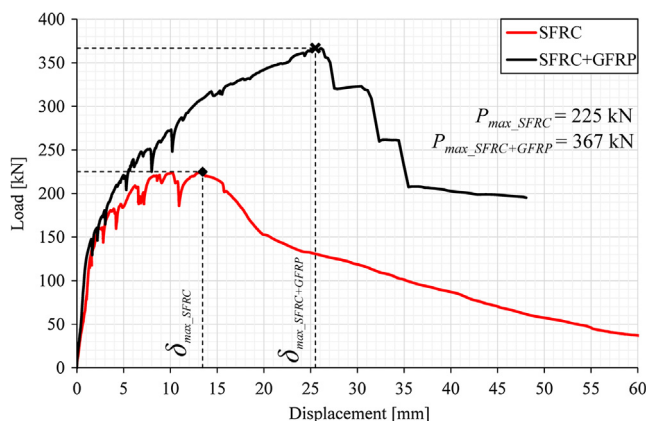


Fig. 16. Bending test. Load - average displacement: comparison between SFRC and SFRC-GFRP segments.

Table 6
Maximum crack widths: comparison.

Load [kN]	Crack width [mm]						
	125	160	180	210	222	250	270
Crack n.	< 0.05	0.15	0.35	0.60	1.00	n/a**	n/a**
SFRC	< 0.05	0.15	0.35	0.60	1.00	n/a**	n/a**
SFRC + GFRP	< 0.05	0.10	0.15	n/a*	0.35	0.45	0.70

n/a* = measure not available since the crack width was not recorded at this load step.

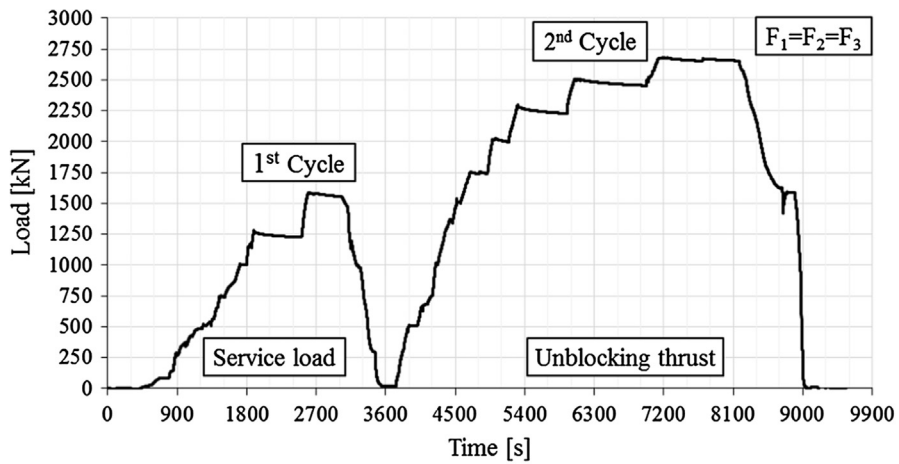
n/a** = measure not available since the segment did not reach this load value.

to 0.25 mm (Table 8).

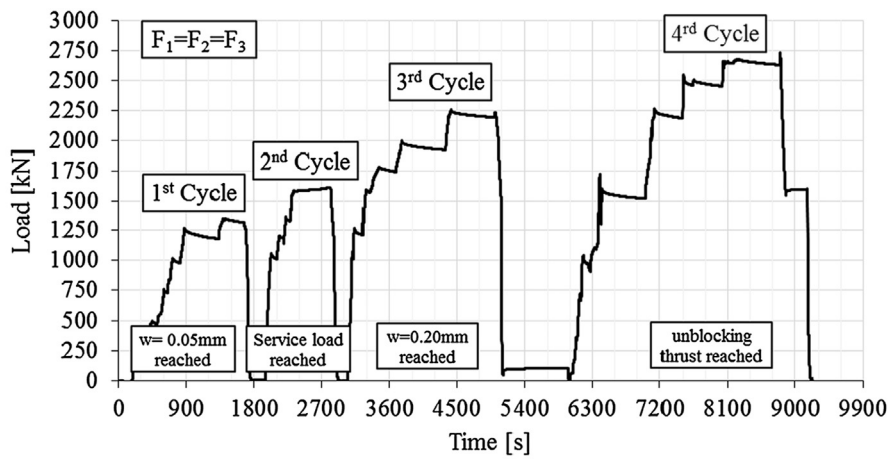
During the unloading phase, the crack widths were measured for load level of 1580 kN, at the end of the test (complete unloading), and after 2 h from the test and are reported in Table 8.

5.3. Point load test: Comparison

Similar patterns of cracks were registered, during the point load tests, for both the solutions. The crack widths measured for the segments SFRC and SFRC-GFRP at three significant load steps (related to the first cracking, service load and maximum TBM thrust load), are finally compared in Table 9.



a)



b)

Fig. 17. Point load test: Load (single pad) vs Time; (a) SFRC segment; (b) SFRC-GFRP segment.

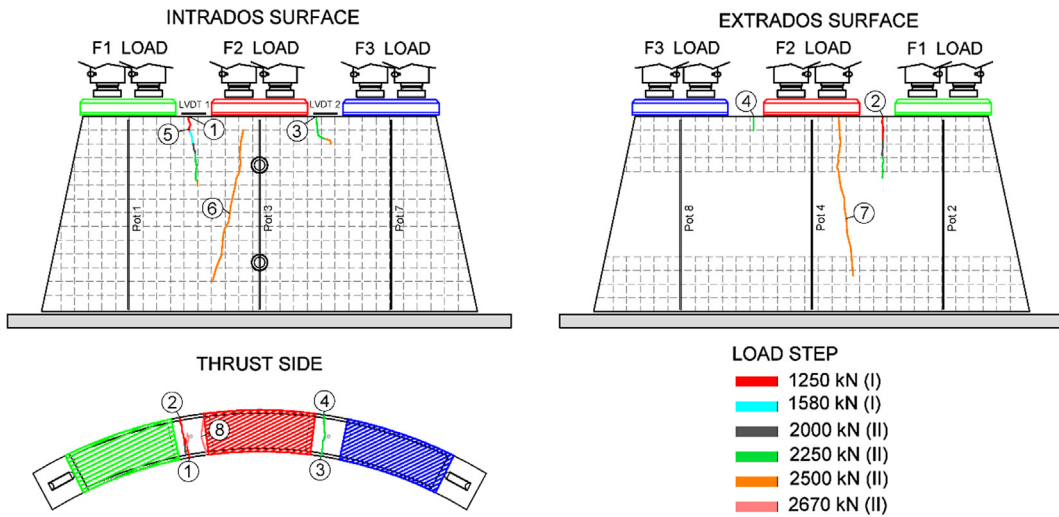


Fig. 18. SFRC Segment. Point load test: Crack pattern.

The addition of the perimetric cage led to halve the crack width under the service load, and to reduce it of about 37.5%, under the unblocking thrust force. Furthermore, a reduction of the crack width of about 33% was measured after the complete unloading.

6. Conclusions

The possibility of adopting a hybrid solution of FRC tunnel segments with GFRP reinforcement is investigated in the paper, through full-scale

Table 7
SFRC Segment. Point load test: crack width. (a) Cycle I; (b) Cycle II.

Phase	Cycle I		
	1250	1580	Unloading
Load [kN]	1250	1580	0
Crack color			
Crack n.	Crack width [mm]		
1	0.05	0.05÷0.10	closed
2	0.05	0.10	closed
3	-	-	-
4	-	-	-
5	-	-	-
6	-	-	-
7	-	-	-
8	-	-	-

Phase	Cycle II										
	Loading								Unloading		
Load [kN]	500	1000	1500	1750	2000	2250	2500	2670	1580	0	
Crack color										after 2h	
Crack n.	Crack width [mm]										
1	closed	0.05	0.05	0.10	0.10	0.15	0.20	0.25	0.25	0.05	<0.05
2	closed	0.05	0.10	0.10	0.10÷0.15	0.30	0.35	0.40	0.40	0.15	0.10÷0.15
3	-	-	-	-	-	0.10	0.10	0.10	0.10	closed	closed
4	-	-	-	-	-	0.05÷0.10	0.05	0.10	0.10	closed	closed
5	-	-	-	-	-	0.25	0.25	0.20	0.2	0.10÷0.15	0.05÷0.10
6	-	-	-	-	-	-	0.1	0.10÷0.15	0.10÷0.15	0.05	0.05
7	-	-	-	-	-	-	0.25	0.25	0.25	0.1	0.1
8	-	-	-	-	-	-	-	<0.05	closed	closed	closed

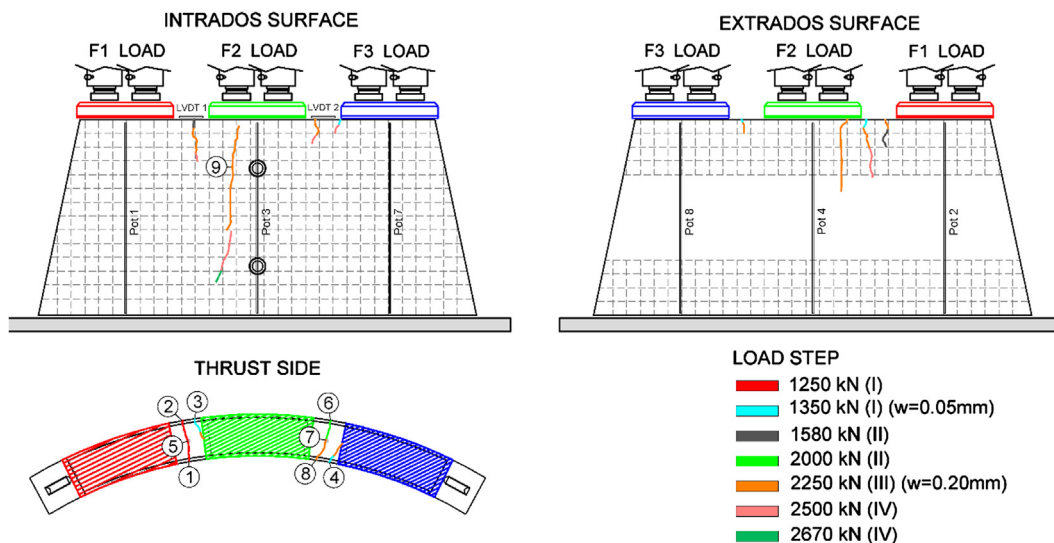


Fig. 19. SFRC-GFRP Segment. Point load test: Crack pattern.

experimental tests. This solution can be useful in those parts of the tunnel (i.e. in cross-passage or shallow tunnel), where, due to bending moment action relevant with respect to the axial force, the FRC only solution cannot satisfy the requirement. The addition of GFRP bars, can be statically effective and can help to overcome the durability problems.

The longitudinal GFRP reinforcement, characterized by a close ring shape, was suitably designed in order to increase the bending resistance of the FRC segment section of about 50%. At this aim 4φ16 rings were placed with perimetric arrangement, typical of hybrid solution.

Two typologies of tests were performed: the flexural one, in order to check the bending capacity of the segments, and the TBM test, in order to simulate the thrust of the TBM machine, during the installation phase. Four FRC full-scale segments were cast, with and without the perimetric GFRP cage, and tested.

The experimental results, presented in the paper, allows to draw the main concluding remarks listed in the following.

1. The results of bending tests, clearly show the synergic effects of the two materials (fibers and GFRP reinforcement) by increasing the peak load and reducing the crack width. Indeed, the design requirement (increase of 50% of the bending resistance) was completely fulfilled, since the hybrid segment exhibited a peak load about 63% higher than the FRC solution. Similar spread of cracks were observed during the tests, with a reduction of the crack width of about 60% in the hybrid segment.
2. The results of the point load test confirm the effectiveness of the solution. Similar cracks patterns are registered during the tests, for both the GFRP-FRC and SFRC segments. In both the cases, firstly splitting cracks formed between the load pads. Finally, at the last

Table 8
SFRC-GFRP Segment. Point load test: crack width.

Phase	Cycle I			Cycle II				
	Loading		Unloading	Loading				Unloading
Load [kN]	1250	1350/0.05	0	1000	1250	1350	1580	0
Crack color								
Crack n.	Crack width [mm]							
1	< 0.05	0.05	closed	< 0.05	< 0.05	< 0.05	0.05	closed
2	< 0.05	0.05	closed	< 0.05	< 0.05	< 0.05	0.05	< 0.05
3	-	0.05	closed	< 0.05	< 0.05	< 0.05	< 0.05	closed
4	-	0.05	closed	< 0.05	< 0.05	< 0.05	< 0.05	closed
5	-	-	-	-	-	-	0.05	closed
6	-	-	-	-	-	-	-	-
7	-	-	-	-	-	-	-	-
8	-	-	-	-	-	-	-	-
9	-	-	-	-	-	-	-	-
10	-	-	-	-	-	-	-	-

Phase	Cycle III						Cycle IV						
	Loading					Unloading	Loading				Unloading		
Load [kN]	1250	1580	1750	2000	2250/0.20	0	1580	2250	2500	2670	1580	0	0
Crack color													after 2h
Crack n.	Crack width [mm]												
1	< 0.05	< 0.05	0.05	0.10	0.10-0.15	0.05	0.10	0.10	0.10	0.15	0.10	< 0.05	< 0.05
2	0.05	0.05	0.05	0.10-0.15	0.10	< 0.05	0.10	0.10	0.15	0.15	0.10	0.05	0.05
3	< 0.05	< 0.05	< 0.05	< 0.05	0.20	0.05	0.15-0.20	0.20	0.25	0.25	0.20	0.10	0.10
4	< 0.05	< 0.05	< 0.05	0.05	0.05	closed	< 0.05	0.05	0.05	0.05	0.05	< 0.05	< 0.05
5	< 0.05	< 0.05	0.05	0.10	0.10	closed	0.05	0.05	0.10	0.10	0.05	< 0.05	< 0.05
6	-	-	-	< 0.05	0.05	< 0.05	0.05	0.05	0.10	0.15	0.10	0.05	0.05
7	-	-	-	-	0.05	closed	0.05	0.10	0.10	0.15	0.10	< 0.05	< 0.05
8	-	-	-	-	0.05	closed	0.05	0.10	0.10	0.10	0.10	0.05-0.10	closed
9	-	-	-	-	0.10	< 0.05	0.05	0.15	0.15	0.20	0.10	0.10	0.10
10	-	-	-	-	0.10	< 0.05	0.15	0.20	0.20	0.25	0.20	0.10	0.10

Table 9
Maximum crack widths: comparison.

	Load [kN]			Unload [kN]
	1st crack	Service load	Unblocking thrust*	
Reinforcement	1250	1580	2670	0
	Maximum crack width [mm]			
SFRC	0.05	0.10	0.40	0.15
SFRC + GFRP	< 0.05	0.05	0.25	0.10

Note: *For metro tunnel, TBM pushing capacity coincides with unblocking thrust.

loading steps a bursting crack open, also. Nevertheless, the addition of the perimetric cage led to halve the crack width under the service load, and to reduce it under the unblocking thrust force, and at the complete unloading, respectively.

References

Almusallam, T.H., Al-Salloum, Y.A., 2006. Durability of GFRP rebars in concrete beams under sustained loads at severe environments. *J. Compos. Mater.* 40 (7), 623–637.

Alsayed, S.H., Al-Salloum, Y.A., Almusallam, T.H., 2000. Performance of glass fiber reinforced plastic bars as a reinforcing material for concrete structures. *Compos. Part B: Eng.* 31 (6–7), 555–567.

Benmokrane, B., Chaallal, O., Masmoudi, R., 1995. Glass fibre reinforced plastic (GFRP) rebars for concrete structure. *Constr. Build. Mater.* 9 (6), 353–364.

Caratelli, A., Meda, A., Rinaldi, Z., Romualdi, P., 2011. Structural behaviour of precast tunnel segments in fiber reinforced concrete. In: *Tunnelling and Underground Space Technology*. Elsevier, pp. 284–291.

Caratelli, A., Meda, A., Rinaldi, Z., 2012. Design according to MC2010 of a fibre-reinforced concrete tunnel in Monte Lirio, Panama. *Struct. Concr.* 13 (3), 166–173.

Caratelli, A., Meda, A., Rinaldi, Z., Spagnuolo, S., 2016. Precast tunnel segments with GFRP reinforcement. *Tunn. Undergr. Space Technol.* 60, 10–20 (November).

Caratelli, A., Meda, A., Rinaldi, Z., Spagnuolo, S., Maddaluno, Giona, 2017. Optimization of GFRP reinforcement in precast segments for metro tunnel lining. *Compos. Struct.* 181, 336–346.

Chen, Y., Davalos, J.F., Kim, H.-Y., 2007. Accelerated aging tests for evaluations of durability performance of FRP reinforcing bars for concrete structures. *Compos. Struct.* 78, 101–111 (March).

CNR-DT 203/2006: “Guide for the Design and Construction of Concrete Structures

Reinforced with Fiber-Reinforced Polymer Bars”, Rome, June, 2007 CNR – Advisory Committee on Technical Recommendations for Construction.

Coccia, S., Meda, A., Rinaldi, Z., 2015. On shear verification according to the fib Model Code 2010 in FRC elements without traditional reinforcement. *Struct. Concr.* 16 (4), 518–523.

Coccia, S., Meda, A., Rinaldi, Z., Spagnuolo, S., 2017. Influence of GFRP skin reinforcement on the crack evolution in RC ties. *Compos. B* 119, 90–100.

Cosenza, E., Manfredi, G., Realfonzo, R., 1997. Behavior and modeling of bond of FRP rebars to concrete. *J. Compos. Constr.* 1 (2), 40–51.

De la Fuente, A., Pujadas, P., Blanco, A., Aguado, A., 2012. Experiences in Barcelona with the use of fibres in segmental linings. *Tunn. Undergr. Space Technol.* 27 (1), 60–71.

Di Carlo, F., Meda, A., Rinaldi, Z., 2016. Design procedure of precast fiber reinforced segments for tunnel lining construction. *Struct. Concr.* 17 (5,1), 747–759.

Ding, Y., Ning, X., Zhang, Y., Pacheco-Torgal, F., Aguiar, J.B., 2014. Fibres for enhancing of the bond capacity between GFRP rebar and concrete. *Constr. Build. Mater.* 51, 303–312.

fib Model Code for Concrete Structures 2010. (2013). Ernst &Sohn.

fib Bulletin No. 83. (2017). Precast tunnel segments in fibre-reinforced concrete.

Issa, M.S., Metwally, I.M., Elzeiny, S.M., 2011. Influence of fibers on flexural behavior and ductility of concrete beams reinforced with GFRP rebars. *Eng. Struct.* 33, 1754–1763.

Kasper, T., Edvardsen, C., Wittneben, G., Neumann, D., 2008. Lining design for the district heating tunnel in Copenhagen with steel fibre reinforced concrete segments. *Tunn. Undergr. Space Technol.* 23 (5), 574–587.

Kim, B., Doh, J.-H., Yi, C.-K., Lee, J.-Y., 2013. Effects of structural fibers on bonding mechanism changes in interface between GFRP bar and concrete. *Compos. B* 45, 768–779.

Liao, L., De La Fuente, A., Cavalaro, S., Aguado, A., 2015. Design of FRC tunnel segments considering the ductility requirements of the Model Code 2010. *Tunn. Undergr. Space Technol.* 47, 200–210.

Meda, A., Rinaldi, Z., Caratelli, A., Cignitti, F., 2016. Experimental investigation on precast tunnel segments under TBM thrust action. *Eng. Struct.* 119, 174–185.

Micelli, F., Nanni, A., 2004. Durability of FRP rods for concrete structures. *Constr. Build. Mater.* 18 (7), 491–503.

Nanni, A. (Ed.), 1993. *Fiber-Reinforced-Plastic (GFRP) Reinforcement for Concrete Structures: Properties and applications*. Elsevier Science. *Developments in Civil Engineering*, pp. 450.

Plizzari, G.A., Tiberti, G., 2008. Steel fibers as reinforcement for precast tunnel segments. *Tunn. Undergr. Space Technol.* 21 (3–4).

Qin, R., Zhou, A., Lau, D., 2017. Effect of reinforcement ratio on the flexural performance of hybrid FRP reinforced concrete beams. *Compos. B* 108, 200–209.

Spagnuolo, S., Meda, A., Rinaldi, Z., Nanni, A., 2017. Precast concrete tunnel segments with GFRP reinforcement. *J. Compos. Construct.* ASCE 21 (5).

Spagnuolo, S., Meda, A., Rinaldi, Z., Nanni, A., 2018. Curvilinear GFRP bars for tunnel segments applications. *Compos. B* 141, 137–147.

Wang, H., Belarbi, A., 2011. Ductility characteristics of fiber-reinforced-concrete beams reinforced with FRP rebars. *Constr. Build. Mater.* 25, 2391–2401.

- Wang, H., Belarbi, A., 2013. Flexural durability of FRP bars embedded in fiber-reinforced-concrete. *Constr. Build. Mater.* 44, 541–550.
- Wona, J.P., Park, C.G., Kim, H.H., Lee, S.W., Jang, C.I., 2008. Effect of fibers on the bonds between FRP reinforcing bars and high-strength concrete. *Compos. B* 39, 747–755.
- Yang, J.M., Min, K.H., Shih, H.O., Yoon, Y.S., 2012. Effect of steel and synthetic fibers on flexural behavior of high-strength concrete beams reinforced with FRP bars. *Compos. B* 43, 1077–1086.
- Yoo, D.-Y., Kwon, K.-Y., Park, J.-J., Yoon, Y.-S., 2015. Local bond-slip response of GFRP rebar in ultra-high-performance fiber-reinforced concrete. *Compos. Struct.* 120, 53–64.